ISSN 1674-1056
http://cpb.iphy.ac.cn
http://iopscience.iop.org/cpb
中国物理 B
Chinese Physics
中国物理
Chinese Physics B

# Spatiotemporal Bloch states of a spin-orbit coupled Bose-Einstein condensate in an optical lattice

Ya-Wen Wei(魏娅雯), Chao Kong(孔超), Wen-Hua Hai(海文华)

**Citation:**Chin. Phys. B . 2019, 28(5): 056701. **doi:** 10.1088/1674-1056/28/5/056701
Journal homepage: http://cpb.iphy.ac.cn; http://iopscience.iop.org/cpb

**What follows is a list of articles you may be interested in**

---

## Current-phase relations of a ring-trapped Bose-Einstein condensate with a weak link

Xiu-Rong Zhang(张秀荣), Wei-Dong Li(李卫东)
Chin. Phys. B . 2019, 28(1): 010303. **doi:** 10.1088/1674-1056/28/1/010303

## Phase diagram and collective modes in Rashba spin–orbit coupled BEC: Effect of in-plane magnetic field

Dong Dong, Zou Xu-Bo, Guo Guang-Can
Chin. Phys. B . 2015, 24(7): 076701. **doi:** 10.1088/1674-1056/24/7/076701

## A space-dependent atomic superfluid current in Bose-Einstein condensates

Li Fei, Li Yong-Fan, Zhang Ping-Ke, Ai Zhen-Zhou, Wu Chang-Yi
Chin. Phys. B . 2015, 24(4): 046701. **doi:** 10.1088/1674-1056/24/4/046701

## Extended Bose–Hubbard model with pair hopping on triangular lattice

Wang Yan-Cheng, Zhang Wan-Zhou, Shao Hui, Guo Wen-An
Chin. Phys. B . 2013, 22(9): 096702. **doi:** 10.1088/1674-1056/22/9/096702

## Production of $^{87}$Rb Bose-Einstein condensates in a hybrid trap

Duan Ya-Fan, Jiang Bo-Nan, Sun Jian-Fang, Liu Kang-Kang, Xu Zhen, Wang Yu-Zhu
Chin. Phys. B . 2013, 22(5): 056701. **doi:** 10.1088/1674-1056/22/5/056701

---

# Spatiotemporal Bloch states of a spin–orbit coupled Bose–Einstein condensate in an optical lattice*

Ya-Wen Wei(魏娅雯), Chao Kong(孔超), and Wen-Hua Hai(海文华)†

*Department of Physics and Key Laboratory of Low-dimensional Quantum Structures and Quantum Control of Ministry of Education, and Synergetic Innovation Center for Quantum Effects and Applications, Hunan Normal University, Changsha* 410081, *China*

(Received 31 October 2018; revised manuscript received 6 February 2019; published online 4 April 2019)

We study the spatiotemporal Bloch states of a high-frequency driven two-component Bose–Einstein condensate (BEC) with spin–orbit coupling (SOC) in an optical lattice. By adopting the rotating-wave approximation (RWA) and applying an exact trial-solution to the corresponding quasistationary system, we establish a different method for tuning SOC via external field such that the existence conditions of the exact particular solutions are fitted. Several novel features related to the exact states are demonstrated; for example, SOC leads to spin–motion entanglement for the spatiotemporal Bloch states, SOC increases the population imbalance of the two-component BEC, and SOC can be applied to manipulate the stable atomic flow which is conducive to control quantum transport of the BEC for different application purposes.

**Keywords:** Bose–Einstein condensate, spin–orbit coupling, spatiotemporal Bloch state, spin–motion entanglement, stable atomic flow, high-frequency limit

**PACS:** 67.85.Hj, 03.75.Lm, 71.70.Ej, 05.60.Gg **DOI:** 10.1088/1674-1056/28/5/056701

## 1. Introduction

Spin–orbit coupling (SOC), the interaction between the spin and momentum of a quantum particle, is crucial for many important condensed matter phenomena.[1] Due to the ground breaking work of Dresselhaus and Rashba, and the further theories and experiments they initiated,[2–8] the physical relevance of SOC can be found. These results were extended to ultracold atomic systems, where various synthetic SOC can be induced and managed by an external laser field. In particular, SOC has been experimentally realized[9] and theoretically investigated[10–14] for binary mixtures of Bose–Einstein condensate (BEC). The cold atomic systems confined in an optical lattice with SOC have also been widely studied. In the mean-field theory, as a many-body system, a BEC governed by Gross–Pitaevskii equation (GPE) provides an important basis for studying the corresponding physical properties. It is important to find exact solutions[15,16] and analytically perturbed solutions[17–20] to the GPE, which can be used to discuss many physical properties such as the macroscopic quantum (or semi-classical) chaos,[17–22] BEC stability,[23–28] the superfluid velocity and flow density,[29] and the generation of solitons.[26] At present, researchers have obtained some exact stationary solutions to the BEC systems in the quasi-one-dimensional (quasi-1D) Kronig–Penny potential,[30] the optical lattice potential,[24,25,31,32] and the two-dimensional optical lattice potential.[33,34] However, the GPE with nonlinear interactions is not easy to solve in general, since the exact solution can exist only under certain parameter conditions which are hard to find. The BEC system with SOC[35–37] is a more complex nonlinear system which poses a challenge to finding the exact solutions. The high frequency approximation method has been widely used because the corresponding approximate systems can be some exactly solvable quasistationary ones,[38–40] which is called the rotating-wave approximation (RWA) for historical reasons.[38] Recently, by means of the high frequency approximation, the SOC tunability has been investigated theoretically and experimentally.[41,42] The SOC strength can also be adjusted by the magnitude and direction of the Raman laser wave-vector. Here, we are motivated in generation of the exact solutions to such a quasistationary system with SOC, by using a high-frequency external field to adjust and reconstruct the system parameters. Consequently, it is possible to control the physical properties of the system and to make quantum transitions between the different analytical quantum states.

The spin–motion entangled state of a single atom has been defined well and was employed in many previous works,[43–45] which contains the well-known Schrödinger cat state[46] $|\Psi(t)\rangle = \frac{1}{\sqrt{2}}(|x_1\rangle|\uparrow\rangle + |x_2\rangle|\downarrow\rangle)$ with the spin-up and spin-down internal states $|\uparrow\rangle$ and $|\downarrow\rangle$ and the coherent motional states $|x_i\rangle$. For a spin–orbit (SO) coupled BEC trapped in a superlattice, the similar spin–motion entangled states can be precisely defined by using two linearly independent motional states to replace the coherent motional states $\frac{1}{\sqrt{2}}|x_i\rangle$.[47] In the full-quantum treatment, these spin–motion entangled states may be implemented to encode the qubits,[43–45,48] and the quantum information can be transported through the spin-dependent currents.[49,50] Therefore, we are also interested in

*Project supported by the National Natural Science Foundation of China (Grant No. 11475060).

†Corresponding author. E-mail: whhai2005@aliyun.com

© 2019 Chinese Physical Society and IOP Publishing Ltd 

how to generate the spin–motion entanglement and to manipulate the spin-dependent currents by tuning the SOC strength and other parameters.[41,42]

In this paper, we consider a SO-coupled BEC driven by a high-frequency field and confined in an optical lattice, through which we study the spatiotemporal Bloch states[51] and the associating physical properties. First, based on the RWA, such a driven system is approximated by a quasistationary one and the relating exact spatiotemporal Bloch states to the latter system are obtained. We analytically show that the SOC strength can be adjusted by the high-frequency field, such that the existence conditions of the exact particular solutions are met. Meanwhile, we find that the parameter regions on the SOC-strength vs. lattice-strength plane for the existence of the exact solution enlarge with the increase in Rabi coupling strength. Then, we show the periodic distribution of the atomic number density, which contains the discrete zero points, corresponding to the instability.[28] Furthermore, we analytically and numerically demonstrate several novel features related to the exact states: (i) the SOC leads to that the spatiotemporal Bloch states become the spin–motion entangled states; (ii) the SOC influences the population imbalance between two BEC components and may result in that all the atoms completely occupy one of the hyperfine states; and (iii) the SOC can be applied to manipulate the stable atomic flow, which is conducive to avoid instability and to control quantum transport of the BEC for different application purposes.[52,53]

## 2. Exact solutions to the quasi-stationary system

We consider a BEC confined in a quasi-1D optical lattice potential $V(x)$ oriented in the longitudinal $x$ direction, and the transverse dynamics of the condensate is assumed to be frozen to the respective ground states of the harmonic traps. In the case of high-frequency driving, the macroscopic quantum state of the BEC is $|\Psi(x,t)\rangle = \Psi_1(x,t)|\uparrow\rangle + \Psi_2(x,t)|\downarrow\rangle$ with the spin-up and spin-down internal states $|\uparrow\rangle$ and $|\downarrow\rangle$ and the macroscopic wave function $\Psi_j(x,t) = \langle x|\Psi_j(t)\rangle$, which is governed by the nonlinear GP equations[54]

$$\begin{aligned} \mathrm{i}\frac{\partial \Psi_j}{\partial t} &= \left[-\frac{1}{2}\frac{\partial^2}{\partial x^2} + V(x)\right]\Psi_j + \mathrm{i}(-1)^j\gamma\frac{\partial \Psi_j}{\partial x} \\ &\quad + \Gamma\Psi_{3-j} + (g|\Psi_j|^2 + g_{12}|\Psi_{3-j}|^2)\Psi_j \\ &\quad + \xi x\sin(\omega t)\Psi_j, \quad j = 1,2, \end{aligned} \tag{1}$$

where the optical lattice potential $V(x) = V_0\sin^2 x$. All the terms in Eq. (1) are the same as the corresponding terms in Ref. [54], except for the driving term. The SOC and Rabi coupling have been realized experimentally,[9] and the driving can be realized experimentally by using a periodic magnetic field gradient applied along the $x$ direction.[55,56] However, the system of units that we have adopted is different. Here, the driving frequency $\omega$ and energies (including the lattice depth $V_0$ and Rabi-coupling strength $\Gamma$) have been normalized in units of the recoil frequency $\omega_\mathrm{r} = \frac{\hbar k^2}{m}$ and recoil energy $E_\mathrm{r} = \hbar\omega_\mathrm{r}$, with $m$ and $k$ being the atomic mass and the standing wave vector. The spatial coordinate $x$, time $t$, and atomic number density $|\Psi_j|^2$ have also been normalized in units of $k^{-1}$, $\omega_\mathrm{r}^{-1}$, and $k$, respectively. The lattice tilt $\xi$ and SOC strength $\gamma > 0$ are in units of $kE_\mathrm{r}$ and $E_\mathrm{r}/k$, respectively, and the constants $g$ and $g_{12}$ are the corresponding dimensionless intra- and inter-species interaction strengths which can be adjusted independently by the optical and magnetic Feshbach-resonance techniques[57,58] in actual experiments. By the high-frequency limit and strong field we mean that the driving frequency and strength obey $\omega \gg 1$ and $\xi/\omega \sim 1$. Due to the particle-number conservation, we let the average total number $N_\mathrm{t} = N_1 + N_2$ of particles in each well be a constant with $N_j$ being the average atomic number per well of the $j$-th component. To make use of the RWA, we seek the wave functions in the form $\Psi_j(x,t) = \Phi_j(x,t)\,\mathrm{e}^{-\mathrm{i}2\frac{\xi}{\omega}x\sin^2(\frac{\omega t}{2})}$ with $\Phi_j(x,t)$ being treated as a slowly varying function of time.[38–40] Inserting such wave functions into Eq. (1) yields the equations

$$\begin{aligned} \mathrm{i}\frac{\partial \Phi_j(x,t)}{\partial t} &= -\frac{1}{2}\frac{\partial^2 \Phi_j(x,t)}{\partial x^2} + \mathrm{i}\left[\gamma(-1)^j + \frac{\xi}{\omega}\right]\frac{\partial}{\partial x}\Phi_j(x,t) \\ &\quad + V(x)\Phi_j(x) + \Gamma\Phi_{3-j}(x,t) \\ &\quad + (g|\Phi_j|^2 + g_{12}|\Phi_{3-j}|^2)\Phi_j(x,t) \\ &\quad + \left[\frac{\gamma(-1)^j\xi}{\omega} + \frac{3\xi^2}{4\omega^2}\right]\Phi_j(x,t) \end{aligned} \tag{2}$$

without driving, where we have replaced the fast-varying functions $\sin^2(\omega t/2)$ and $\sin^4(\omega t/2)$ by their average values $1/2$ and $3/8$, respectively, according to the RWA. By substituting the stationary solutions

$$\Phi_j(x,t) = \psi_j(x)\,\mathrm{e}^{-\mathrm{i}\mu t} \tag{3}$$

with chemical potential $\mu$ into Eq. (2), we obtain the time-independent equations of $\psi_j(x)$

$$\begin{aligned} \mu_j\psi_j &= -\frac{1}{2}\psi_{j,xx} + \mathrm{i}\gamma_j\psi_{j,x} + \Gamma\psi_{3-j} + V(x)\psi_j \\ &\quad + (g|\psi_j|^2 + g_{12}|\psi_{3-j}|^2)\psi_j, \\ \gamma_j &= (-1)^j\gamma + \frac{\xi}{\omega}, \quad \mu_j = \mu - (-1)^j\gamma\frac{\xi}{\omega} - \frac{3\xi^2}{4\omega^2}, \end{aligned} \tag{4}$$

with $\gamma_j$ and $\mu_i$ being the recombined SOC strengths and chemical potentials, which are tuned by the driving parameter ratio $\xi/\omega$.

It is worth noting that for $\gamma = 0$ and $\Gamma = 0$, equation (4) is reduced to the basic equations in Ref. [31], and the corresponding exact solutions have been constructed. The presence of SOC and Rabi coupling makes the system more complicated and more difficult to solve. However, according to the famous Floquet theorem, there exists an exact Bloch solution

to a spatially periodic system.[51] In fact, if we adjust the driving parameter ratio $\xi/\omega$ and SOC strength $\gamma$ to satisfy the following conditions:

$$\mu = \frac{1}{2}\left[1+N_{\rm t}(g+g_{12})+V_0+\frac{3}{2}(\Gamma^2+\gamma^2)\right],$$
$$\frac{\xi^2}{\omega^2} = \Gamma^2+\gamma^2, \tag{5}$$

then the exact particular solutions to the spatially periodic Eq. (4) can be obtained by inserting the trial Bloch solutions

$$\psi_j = a_j\cos x + {\rm i}b_j\sin x \tag{6}$$

with real undetermined constants $a_j$ and $b_j$ into Eq. (4), and by using the normalization condition. Firstly, the normalization and equation (6) give the average number of particles per well in Eq. (5) as[24,31]

$$N_{\rm t} = N_1+N_2 = \frac{1}{n\pi}\int_{\pi/2}^{(n+1/2)\pi}\sum_{j=1}^{2}|\psi_j|^2\,{\rm d}x = \frac{1}{2}\sum_{j=1}^{2}(a_j^2+b_j^2).$$

Then, by combining Eqs. (6) and (5) with Eq. (4), we derive three pairs of equations

$$g(a_j^2-b_j^2)+g_{12}(a_{3-j}^2-b_{3-j}^2) = V_0,$$
$$a_j^2+b_j^2 = N_{\rm t}-(-1)^j\frac{2\gamma\sqrt{\Gamma^2+\gamma^2}}{g-g_{12}},$$
$$a_j^2-b_j^2 = -\frac{\gamma_{3-j}}{\gamma_j}(a_{3-j}^2-b_{3-j}^2) = \frac{V_0\gamma_{3-j}}{g\gamma_{3-j}-g_{12}\gamma_j}$$

for $j=1,2$. Solving these equations yields the four squares of the undetermined constants. Hereafter, we take the positive constants in the forms

$$a_j = \sqrt{\frac{N_{\rm t}}{2}-(-1)^j\frac{\gamma\sqrt{\Gamma^2+\gamma^2}}{g-g_{12}}+\frac{V_0\gamma_{3-j}}{2(g\gamma_{3-j}-g_{12}\gamma_j)}},$$
$$b_j = \sqrt{\frac{N_{\rm t}}{2}-(-1)^j\frac{\gamma\sqrt{\Gamma^2+\gamma^2}}{g-g_{12}}-\frac{V_0\gamma_{3-j}}{2(g\gamma_{3-j}-g_{12}\gamma_j)}} \tag{7}$$

for $j=1,2$. Making use of Eqs. (5) and (7), we can easily prove that equation (6) is just a pair of exact solutions to Eq. (4). For the fixed parameters $\Gamma$ and $\gamma$, the first condition of Eq. (5) can be satisfied by the undetermined chemical potential and the second condition is adjusted by the driving parameter ratio $\xi/\omega$. The latter condition means that the system (4) with nonzero SOC and/or Rabi strengths has exact solution (6), if the ratio $\xi/\omega$ is equal to $\sqrt{\Gamma^2+\gamma^2}$. The result is similar to the well-known result that when the driving parameter ratio coincides with a zero of the zero-order Bessel function, a high-frequency driven two-state model arrives at a particular localized state; namely, the coherent destruction of tunneling.[39,40]

Rewriting Eq. (6) in its exponential form

$$\psi_j = R_j(x)\exp[{\rm i}\Theta_j(x)],\quad j=1,2,$$
$$R_j = \sqrt{a_j^2+(b_j^2-a_j^2)\sin^2 x},$$
$$\Theta_j = \arctan\frac{b_j\sin x}{a_j\cos x} = \int\frac{a_jb_j}{R_j^2}\,{\rm d}x, \tag{8}$$

and applying Eq. (7) to Eq. (8) leads to the atomic number densities

$$R_j^2 = \frac{1}{2}\left[N_{\rm t}+\frac{V_0\gamma_{3-j}\cos(2x)}{g\gamma_{3-j}-g_{12}\gamma_j}-(-1)^j\frac{2\gamma\sqrt{\Gamma^2+\gamma^2}}{g-g_{12}}\right]. \tag{9}$$

Clearly, the exact solutions in Eq. (8) have the similar forms with those in Refs. [24] and [31] and in Refs. [24]–[26] and [28] with zero elliptic modulus for the spatially periodic nonlinear systems without SOC. However, to construct such a solution to system (4) with SOC, the high-frequency driving with the parameters obeying Eq. (5) must be applied. Given Eq. (8), we can calculate the average atomic numbers per well as[24,31]

$$N_j = \frac{1}{n\pi}\int_{\pi/2}^{(n+1/2)\pi}R_j^2\,{\rm d}x = \frac{N_{\rm t}}{2}-(-1)^j\frac{\gamma\sqrt{\Gamma^2+\gamma^2}}{g-g_{12}}. \tag{10}$$

To keep the positive semidefinite property of the atomic number densities, $|\psi_j|^2 = R_j^2 \geq 0$ for any $x$ value, from Eq. (9) we have the necessary and sufficient conditions[31]

$$|V_0| \leq V_{\rm c} = \min\{V_{1{\rm c}},V_{2{\rm c}}\},$$
$$V_{j{\rm c}} = \left|\frac{g\gamma_{3-j}-g_{12}\gamma_j}{\gamma_{3-j}}\right|\left[N_{\rm t}-(-1)^j\frac{2\gamma\sqrt{\Gamma^2+\gamma^2}}{g-g_{12}}\right]. \tag{11}$$

The exact solutions Eqs. (6) and (7) to the quasistationary Eq. (4) are valid if and only if the depth $V_0$ of the lattice potential obeys the constraint relation Eq. (11). According to Eq. (10), we know that the quantity in the square brackets is greater than zero due to $N_j \geq 0$ for any $j$, which gives a limit to the maximal value of $\gamma$ for a set of fixed other parameters. Therefore, for $g-g_{12}>0$ or $g-g_{12}<0$, equation (11) gives $V_{\rm c}=V_{2{\rm c}}$ or $V_{\rm c}=V_{1{\rm c}}$, respectively. Without loss of generality, we can suppose $V_0 \geq 0$. Then, based on Eq. (11), taking the parameters $N_{\rm t}=10$, $g=0.6$, and $g_{12}=0.1$, we plot the boundary curves $V_0=V_{2{\rm c}}(\gamma)$ for the parameter regions of the exact solution under the RWA as a function of $\gamma$ for $\Gamma=0.6$, 0.8, and 1.4, respectively, as shown in Fig. 1(a). Any curve in Fig. 1(a) with a fixed $\Gamma$ value gives a boundary corresponding to the parameter regions for the existence and nonexistence of the exact solution (6). Noticing the sign "$\leq$" in Eq. (11), the parameter regions of exact solution (6) are $A$, $(A+B)$, and $(A+B+C)$ for $\Gamma=1.4$, 0.8, and 0.6, respectively, which means that the stronger Rabi coupling increases the size of the considered parameter region. In Fig. 1(b) based on $V_0=V_{1{\rm c}}(\gamma)$, we also show the existence regions of the exact solution for $N_{\rm t}=8$ and different nonlinear interaction strengths $g=0.1$ and $g_{12}=0.6$. Similar to Fig. 1(a), the parameter regions for the existence of the exact solution still are $A$, $(A+B)$, and $(A+B+C)$ for $\Gamma=1.4$, 0.8, and 0.6, respectively. The existence regions enlarge with the increase in Rabi coupling strength $\Gamma$. For any set

of the considered parameters, in the two regions labeled $D$, the exact solution (6) cannot exist. All the curves in Fig. 1 monotonically decrease such that for any fixed $\Gamma$ value, the maximal lattice strength associated with the exact solution has to decrease with increasing SOC strength. Comparing Fig. 1(a) with Fig. 1(b), we can see that increasing the average atomic number $N_t$ per well can enlarge the region area existing exact solution for a set of fixed parameters.

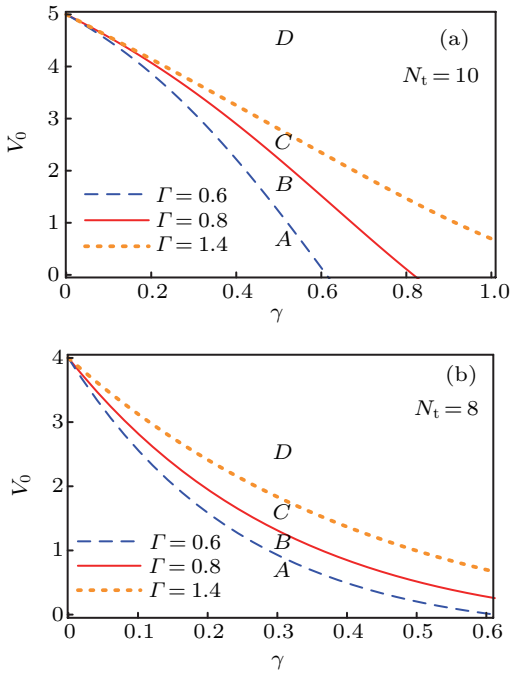



**Fig. 1.** Lattice depth $V_0$ versus SOC strength $\gamma$ for different parameters $\Gamma$, (a) $N_t = 10$, $g = 0.6$, $g_{12} = 0.1$, and (b) $N_t = 8$, $g = 0.1$, $g_{12} = 0.6$. The parameter plane is divided into different regions by the boundary curves, which are labeled by $A$, $B$, $C$, and $D$. Hereafter, all the quantities plotted in the figures are dimensionless.

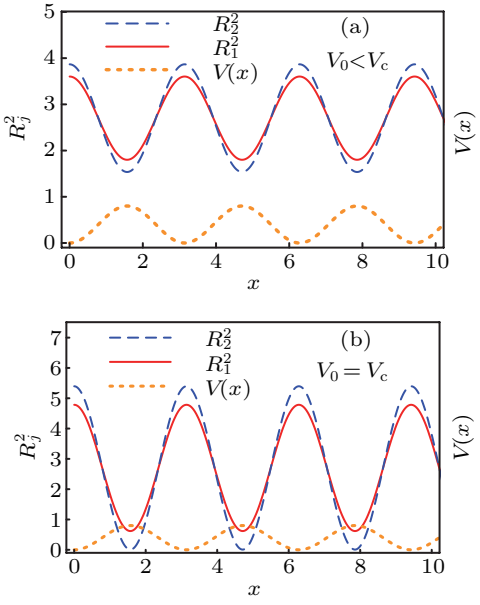



**Fig. 2.** Spatial distributions of the atomic number density and potential function for (a) $V_0 = 0.8$ obeying $V_0 < V_c$ and (b) $V_0 = 1.57839$ corresponding to $V_0 = V_c$. The atomic number density exhibits different periodic distributions without zero point in (a) and with zero points in (b). Both figures show that every peak of the number densities aligns to a potential well.

From Eq. (9), we show the spatial distributions of the atomic number density $R_j^2(x)$ and the lattice potential $V(x)$ for the parameters $g = 0.6$, $g_{12} = 0.2$, $\gamma = 0.1$, $N_t = 5$, $\Gamma = 0.8$, and $V_0 = 0.8 < V_c$ in Fig. 2(a), $V_0 = 1.57839 = V_c$ in Fig. 2(b). When $V_0 < V_c$ is set, although the atomic number densities have different spatial distributions in Fig. 2(a), their maxima always align to the center points of the potential wells, and the atomic number density is greater than zero at any spatial position. This means that more atoms are distributed around the centers of the potential wells, corresponding to the higher stability of the BEC system compared to that of the case where the density peaks align to potential barrier sites and some zero density points exist. In the case of $V_0 = V_c$, figure 2(b) shows that $R_j^2$ maybe zero at the peak sites of the potential.

## 3. Physics related to the spatiotemporal Bloch states

By applying the existence conditions of the considered exact solutions to Eq. (4) and the corresponding parameter regions, we have established the exact particular solutions (6) and (7), and illustrated the associated atomic number densities. In this section, we will demonstrate that the obtained states are just the spatiotemporal Bloch states and reveal some physical properties of the BEC system in such states.

We first demonstrate that the obtained states are just the spatiotemporal Bloch states. From Eq. (6), we rewrite the exact solutions as $\psi_j = F_j(x)\,\mathrm{e}^{-\mathrm{i}x}$, $F_j(x) = \frac{1}{2}[a_j(1+\mathrm{e}^{\mathrm{i}2x}) - b_j(1-\mathrm{e}^{\mathrm{i}2x})]$ for $j = 1,2$. Clearly, these are two Bloch solutions to Eq. (4) with the Bloch wave vector $-1$ and Bloch state functions $F_j(x)$ which possess the same period with the potential $V(x)$. Then from the macroscopic quantum state $|\Psi(t)\rangle = |\Psi_1(t)\rangle|\uparrow\rangle + |\Psi_2(t)\rangle|\downarrow\rangle$ and Eq. (3), we have the space–time dependent state

$$\begin{aligned} |\Psi(x,t)\rangle &= \langle x|\Psi(t)\rangle = |F(x,t)\rangle\,\mathrm{e}^{-\mathrm{i}\mu t}, \\ |F(x,t)\rangle &= [F_1(x)|\uparrow\rangle + F_2(x)|\downarrow\rangle]\,\mathrm{e}^{-\mathrm{i}x\left[1+\frac{2\xi}{\omega}\sin^2\left(\frac{\omega t}{2}\right)\right]} \end{aligned} \quad (12)$$

in the coordinate representation. Obviously, equation (12) is a Floquet solution to Eq. (1) with the Floquet quasienergy $-\mu$ and Floquet state $|F(x,t)\rangle$ of the same period with the driving force. At any fixed time, equation (12) is an usual Bloch state. Because the considered system is a time–space periodic system, we call Eq. (12) the spatiotemporal Bloch state.[51] The motional state functions $F_j(x)$ contain the constants $a_j$ and $b_j$ with some arbitraries, so varying these constants can produce different spatiotemporal Bloch states.

We then show that SOC leads to generation of spin–motion entanglement. Quantum entanglement is a universal but very special kind of quantum state in the multi-particle system. In previous work, for a SO-coupled BEC trapped in a superlattice, Kong *et al.* have studied the spatially chaoticity-dependent spin–motion entanglement.[47] Here we study the

effects of SOC on the chaoticity-independent spin–motion entanglement between internal hyperfine (pseudospin) states and external motional (orbit) states. From Eq. (7), we observe that the constants in exact solution (6) to the quasistationary Eq. (4) obey $a_1 = a_2$ and $b_1 = b_2$ only if $\gamma = 0$. Consequently, the two motional states in Eq. (12) become the same, $F_1(x) = F_2(x)$, such that the quantum state $|\Psi(x,t)\rangle$ can be separated as the direct product between the spin part and motional part and become an unentangled state. The nonzero SOC strength makes the different and linearly independent motional states in Eq. (12) and leads to the spin–motion entanglement. The orbital part of the spin–motion entangled state can be used to manipulate the qubits for quantum information processing with spins.

We now investigate the population imbalance of the two-component BEC. Given Eq. (10), the difference between the average atomic numbers reads $N_1 - N_2 = 2\gamma\sqrt{\Gamma^2+\gamma^2}/(g-g_{12})$, which is called the population imbalance of the two-component BEC. The zero SOC strength $\gamma = 0$ results in balance with the same average number per well $N_1 = N_2$ and causes the entanglement loss. In the presence of SOC. for $g - g_{12} > 0$, we have $N_1 > N_2$ so equation (10) implies that only $N_2$ may reach zero with a large enough SOC strength. In contrast, the case $g - g_{12} < 0$ means that only $N_1$ may reach zero. In Fig. 3, based on Eq. (10), we take Rabi coupling strength $\Gamma = 0.1$ and average atomic number $N_t = 5$ to plot the population imbalance $N_1 - N_2$ versus SOC strength $\gamma$ for $g = 0.6$, $g_{12} = 0.2$ (solid curve), and $g = 0.2$, $g_{12} = 0.6$ (dotted curve). Clearly, the population imbalance monotonically increases or decreases with the increase in SOC strength for the case $g - g_{12} > 0$ or the case $g - g_{12} < 0$, respectively. When the SOC strength arrives at $\gamma \approx 0.99750313$, we obtain $N_1 - N_2 = N_t = 5$ or $N_1 - N_2 = -N_t = -5$ associated with $N_2 = 0$ or $N_1 = 0$. Thus, all the atoms are completely populated on one of the hyperfine states, as shown in Fig. 3. The results reveal the population transfer between the two BEC components by adjusting the SOC strength.

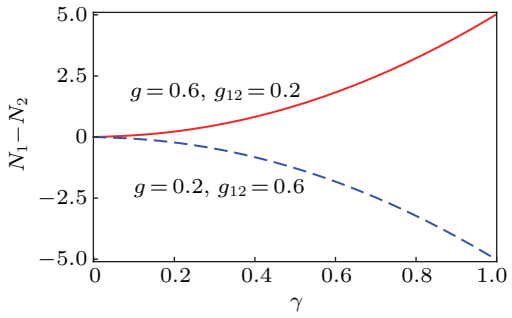



**Fig. 3.** The population imbalance $N_1 - N_2$ as a function of the SOC strength $\gamma$ for the parameters $\Gamma = 0.1, N_t = 5$, and $g = 0.6, g_{12} = 0.2$ (solid curve), and $g = 0.2, g_{12} = 0.6$ (dashed curve).

Finally, we discuss the establish of the stable superfluid density. Applying Eqs. (7) and (9) to the definitions of the superfluid velocity and density, $v_j(x) = k\hbar\Theta_{jx}/m = k\hbar a_j b_j/(mR_j^2)$, $J_j = R_j^2 v_j = k\hbar a_j b_j/m$, after adopting our dimensionless parameters we obtain the superfluid densities and flow velocities

$$J_{j\pm} = \pm\sqrt{\left[\frac{N_t}{2} - (-1)^j \frac{\gamma\sqrt{\Gamma^2+\gamma^2}}{g-g_{12}}\right]^2 - \left[\frac{V_0\gamma_{3-j}}{2(g\gamma_{3-j} - g_{12}\gamma_j)}\right]^2},$$
$$v_{j\pm}(x) = \frac{J_{j\pm}}{R_j^2(x)}. \tag{13}$$

The constant superfluid densities describe two uniform atom currents for the two BEC components, and can be conveniently manipulated by tuning any one of the experimental parameters $N_t$, $g_{12}$, $g$, $V_0$ and recombined $\gamma$. The signs of $J_j$ determine the directions of the atomic currents, which can be initially set[43–45] when the two species of atoms are loaded in the optical lattices and provide the persistent incident currents.[52] In Fig. 4, we plot the flow density $J_j$ versus the SOC strength for the parameters $\Gamma = 0.1$, $N_t = 5$, $V_0 = 1$, $g = 0.6$, and $g_{12} = 0.4$. When $J_j$ take the positive sign of Eq. (13), the two arrays of atomic quasi-clusters flow toward the right; when $J_j$ take the negative sign, the atomic quasi-clusters of the two arrays flow to the left. However, when $J_1$ and $J_2$ have different signs, the two arrays of atomic quasi-clusters flow with opposite directions. As shown in Fig. 4, the flow density $J_{1+}$ increases with increasing SOC strength $\gamma$, while $J_{2+}$ decreases with the increase in SOC strength. Conversely, $J_{j-}$ have different increasing trends with $J_{j+}$ for $j = 1, 2$. Interestingly, when we change the SOC strength to $\gamma = 0.702682$, only the superfluid density $J_1$ exists and the second component vanishes, $J_{2\pm} = 0$. From the known research results,[59] when the atomic number density $R_j^2$ does not contain a zero, the BEC system may be stable. In contrast, when $R_j^2$ has a zero point, the system may be unstable for the given parameters.[28,32] This stability is revealed from a different viewing angle in Eq. (13) where the zero density $R_j^2$ is associated with the infinite superfluid velocity resulting in the instability. Therefore, we can establish the stable superfluid currents by avoiding the critical parameter point $V_0 = V_c$ and adopting the parameters in regions obeying $V_0 < V_c$.

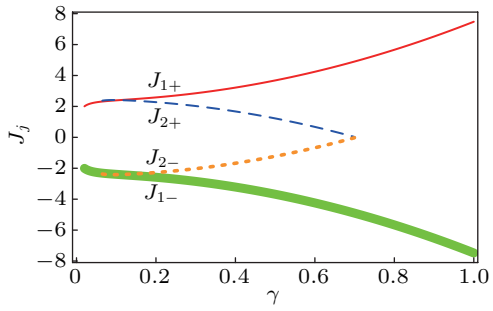



**Fig. 4.** The flow density $J_j$ versus SOC strength $\gamma$. The parameters are chosen as $\Gamma = 0.1$, $N_t = 5$, $V_0 = 1$, $g = 0.6$, and $g_{12} = 0.4$. The superfluid density $J_{1+}$ ($J_{2+}$) increases (decreases) with increasing SOC strength, and conversely for $J_{1-}$ and $J_{2-}$.

In addition, under RWA, we can use the exact solution (6) and the corresponding parameter conditions to come up with some other interesting physical phenomena and properties.

## 4. Discussion and conclusion

In summary, we have researched the spatiotemporal Bloch states and the relating physical properties for a SO-coupled BEC trapped in an optical lattice and driven by a high-frequency field. Based on the widely used RWA method, we obtain the exact solution (6) to the quasistationary equation (4) and the analytical spatiotemporal Bloch state (12). We establish a different method for tuning SOC via external field such that the existence conditions of the exact particular solutions are fitted. From the existence conditions, we find that the parameter region on the plane of lattice-strength vs. SOC-strength can be adjusted by the Rabi coupling strength. As the Rabi coupling strength increases, the regions of the parameters existing exact solutions increase. Then, we show the periodic distributions of the atomic number density which are associated with the stability and instability of the system. When $V_0 < V_c$ is set, more atoms are distributed around the centers of the potential wells without zero point of the atomic number density, corresponding to higher stability of the BEC system. When $V_0 = V_c$ is selected, the atomic number density contains zero points corresponding to the instability. In particular, several new physical features related to the exact states are revealed, as follows. (i) The SOC leads to generation of the spin–motion entanglement in the obtained spatiotemporal Bloch states. In contrast, zero SOC strength results in disappearance of the spin–motion entanglement. The orbital part of the spin–motion entangled state can be used to manipulate the spin qubits for quantum information processing. (ii) Tuning SOC changes the population imbalance between two BEC components and may cause all of the atoms to completely concentrate on one of the hyperfine states. (iii) The SOC can be applied to manipulate the stable atomic flow. For a set of fixed parameters, one component of the superfluid density decreases with the increase in SOC strength, and another component consequently increases.

BEC is a well-controlled collection of atoms that can be used to study new aspects of quantum optics, many-body physics, and superfluidity. It is highly desirable to transport BEC from a stable source to a designated place.[52] The results of this paper provide a method that avoids instability of the system and controls BEC motion via the modulated optical lattice and the tunable SOC, which is particularly conducive to control quantum transport of BEC for different application purposes.[52,53]

## References


[1] Zhang Y P, Mao L and Zhang C W 2012 *Phys. Rev. Lett.* **108** 035302
[2] Elliott R J 1954 *Phys. Rev.* **96** 280
[3] Dresselhaus G, Kip A F and Kittel C 1954 *Phys. Rev.* **95** 568
[4] Dresselhaus G 1955 *Phys. Rev.* **100** 580
[5] Rashba E I 1960 *Sov. Phys. Solid State* **2** 1224
[6] Liu L, Chen W X, Wang R Q and Hu L B 2018 *Chin. Phys. B* **27** 047201
[7] Tang Z H, Yao T X and Liu J J 2017 *Chin. Phys. B* **26** 117203
[8] Zhang L 2018 *Chin. Phys. B* **27** 067203
[9] Lin Y J, Jiménez-García K and Spielman I B 2011 *Nature* **471** 83
[10] Galitski V and Spielman I B 2013 *Nature* **494** 49
[11] Huang F J, Chen Q H, and Liu W M 2014 *Phys. Rev. A* **89** 033624
[12] Xie W F, He Y Z and Bao C G 2015 *Chin. Phys. B* **24** 060305
[13] Yu Z F and Xue J K 2014 *Phys. Rev. A* **90** 033618
[14] Zhang X F, Kato M, Han W, Zhang S G, and Saito H 2017 *Phys. Rev. A* **95** 033620
[15] Liang Z X, Zhang Z D and Liu W M 2005 *Phys. Rev. Lett.* **94** 050402
[16] Li Z J, Hai W H and Deng Y 2013 *Chin. Phys. B* **22** 090505
[17] Hai W H, Lee C H, Chong G S and Shi L 2002 *Phys. Rev. E* **66** 026202
[18] Lee C H, Hai W H, Shi L, Zhu X W and Gao K L 2001 *Phys. Rev. A* **64** 053604
[19] Zhou Z, Hai W H, Deng Y and Xie Q T 2012 *Chaos Solitons & Fractals* **45** 1423
[20] Liu L W, Gengzang D J, An X J and Wang P Y 2018 *Chin. Phys. B* **27** 034205
[21] Abdullaev F K and Kraenkel R A 2000 *Phys. Rev. A* **62** 023613
[22] Fujioka J, Cortés E, Pérez-Pascual R, Rodríguez R F, Espinosa A and Malomed B A 2011 *Chaos* **21** 033120
[23] Xu J, Hai W H and Li H 2007 *Chin. Phys. B* **16** 2244
[24] Bronski J C, Carr L D, Deconinck B and Kutz J N 2001 *Phys. Rev. Lett.* **86** 1402
[25] Deconinck B, Kutz J N, Patterson M S and Warner B W 2003 *J. Phys. A: Math. Gen.* **36** 5431
[26] Kostov N A, Enol'skii V Z, Gerdjikov V S, Konotop V V and Salerno M 2004 *Phys. Rev. E* **70** 056617
[27] Zhang H F, Chen W, Yu C C, Sun L H and Xu D H 2017 *Chin. Phys. B* **26** 080304
[28] Bronski J C, Carr L D, Deconinck B, Kutz J N and Promislow K 2001 *Phys. Rev. E* **63** 036612
[29] Hai W H, Li C H, Fang X M and Gao K L 2004 *Physica A* **335** 445
[30] Theodorakis S and Leontidis E 1997 *J. Phys. A: Math. Gen.* **30** 4835
[31] Hai W H, Li Y, Xia B and Luo X 2005 *Europhys. Lett* **71** 28
[32] Deng H M, Hai W H and Zhu Q Q 2006 *J. Phys. A: Math. Gen.* **39** 49
[33] Deconinck B, Frigyik B A and Kutz J N 2001 *Phys. Lett. A* **283** 177
[34] Hai W H, Chong G S, Xie Q T and Lu J 2004 *Eur. Phys. J. D* **28** 267
[35] Lü H, Zhu S B, Qian J and Wang Y Z 2015 *Chin. Phys. B* **24** 090308
[36] Liu W M and Li J 2018 *Acta Phys. Sin.* **67** 110302 (in Chinese)
[37] Zhang H F, Chen F, Yu C C, Sun L H and Xu D H 2017 *Chin. Phys. B* **26** 080304
[38] Cook R J, Shankland D G and Wells A L 1985 *Phys. Rev. A* **31** 564
[39] Kayanuma Y and Saito K 2008 *Phys. Rev. A* **77** 010101
[40] Yuan L M, Xu Y G, Gao W, Dai F and Wu Q L 2018 *Chin. Phys. B* **27** 044101
[41] Salerno M, Abdullaev F K, Gammal A and Tomio L 2016 *Phys. Rev. A* **94** 043602
[42] Jiménez-García K, LeBlanc L J, Williams R A, Beeler M C, Qu C, Gong M, Zhang C and Spielman I B 2015 *Phys. Rev. Lett.* **114** 125301
[43] Leibfried D, Blatt R, Monroe C and Wineland D 2003 *Rev. Mod. Phys.* **75** 281
[44] Mizrahi J, Senko C, Neyenhuis B, Johnson K G, Campbell W C, Conover C W S and Monroe C 2013 *Phys. Rev. Lett.* **110** 203001
[45] Hai K, Luo Y R, Chong G S, Chen H and Hai W H 2017 *Quantum Inf. Comput.* **17** 456

[46] Monroe C, Meekhof D M, King B E and Wineland D J 1996 *Science* **272** 1131

[47] Kong C, Chen H, Li C L and Hai W H 2018 *Chaos* **28** 023115

[48] Nakamura Y, Pashkin Y A and Tsai J S 1999 *Nature* **398** 786

[49] Romero-Isart O and García-Ripoll J J 2007 *Phys. Rev. A* **76** 052304

[50] Luo Y R, Lu G B, Kong C and Hai W H 2016 *Phys. Rev. A* **93** 043409

[51] Arlinghaus S and Holthaus M 2011 *Phys. Rev. A* **84** 063617

[52] Paul T, Richter K and Schlagheck P 2005 *Phys. Rev. Lett.* **94** 020404

[53] Salger T, Kling S, Hecking T, Geckeler C, Morales-Molina L and Weitz M 2009 *Science* **326** 1241

[54] Cheng Y S, Tang G H and Adhikari S K 2014 *Phys. Rev. A* **89** 063602

[55] Chen Y A, Nascimbéne S, Aidelsburger M, Atala M, Trotzky S and Bloch I 2011 *Phys. Rev. Lett.* **107** 210405

[56] Ma R, Tai M E, Preiss P M, Bakr W S, Simon J and Greiner M 2011 *Phys. Rev. Lett.* **107** 095301

[57] Blatt S, Nicholson T L, Bloom B J, Williams J R, Thomsen J W, Julienne P S and Ye J 2011 *Phys. Rev. Lett.* **107** 073202

[58] Inouye S, Andrews M R, Stengeretal J, Miesner H J, Stamper-Kurn D M and Ketterle W 1998 *Nature* **392** 151

[59] Strecker K E, Partridge G B, Truscott A G and Hulet R G 2002 *Nature* **417** 150